



HHS Public Access

Author manuscript

Comput Methods Biomech Biomed Eng Imaging Vis. Author manuscript; available in PMC
2020 January 01.

Published in final edited form as:

Comput Methods Biomech Biomed Eng Imaging Vis. 2019 ; 7(4): 396–405. doi:
10.1080/21681163.2018.1442751.

Simulation of surface strain in tibiofemoral cartilage during walking for the prediction of collagen fiber orientation

Milad Rakhsha^a, Colin R. Smith^b, Antonio Recuero^a, Scott C. E. Brandon^b, Michael F Vignos^b, Darryl G. Thelen^b, Dan Negrut^a

^aSimulation Based Engineering Laboratory (SBEL), Department of Mechanical Engineering, University of Wisconsin-Madison, Madison, Wisconsin 53706

^bNeuromuscular Biomechanics Laboratory (NMBL), Department of Mechanical Engineering, University of Wisconsin-Madison, Madison, Wisconsin 53706

Abstract

The collagen fibers in the superficial layer of tibiofemoral articular cartilage exhibit distinct patterns in orientation revealed by split lines. In this study, we introduce a simulation framework to predict cartilage surface loading during walking to investigate if split line orientations correspond with principal strain directions in the cartilage surface. The two-step framework uses a multibody musculoskeletal model to predict tibiofemoral kinematics which are then imposed on a deformable surface model to predict surface strains. The deformable surface model uses absolute nodal coordinate formulation (ANCF) shell elements to represent the articular surface and a system of spring-dampers and internal pressure to represent the underlying cartilage. Simulations were performed to predict surface strains due to osmotic pressure, loading induced by walking, and the combination of both loading due to pressure and walking. Time-averaged magnitude-weighted first principal strain directions agreed well with split line maps from the literature for both the osmotic pressure and combined cases. This result suggests there is indeed a connection between collagen fiber orientation and mechanical loading, and indicates the importance of accounting for the pre-strain in the cartilage surface due to osmotic pressure.

Keywords

knee articular cartilage; collagen fibers; principal strains; absolute nodal coordinate formulation (ANCF); deformable mesh contact; superficial zone; fiber orientation

{ rakhsha@wisc.edu, crsmith25@wisc.edu, recuero@wisc.edu, sbrandon2@wisc.edu, mvignos@wisc.edu, dgthelen@wisc.edu, negrut@wisc.edu. }

Supplementary Materials

For completeness, deflection and strain results as presented for the femur (Figure 7) are shown for tibia cartilage in Figure 9. This figure shows the principal strain directions on the tibia at three instants of the gait cycle. Similar to femoral cartilage, tibia cartilage illustrates tensile behavior on the periphery of the contact region, especially at the first peak of the gait loading. However, the periphery of the contact region also exhibited regions with negative first principal strain (Figure 9). We believe that the shape of the tibia cartilage plays a major role in such behavior. Moreover, the numerical split-line patterns are shown in Figure 10. Due to limited availability ($N = 1$) of experimental split line maps for the tibia in literature (Meachim et al., 1974), only our simulated principal strain directions are shown.

Finally, attached to this paper is a video which illustrates the deflection of the femur and tibia cartilages during the gait cycle, along with the maximum principal strain.

Introduction

During everyday movements such as walking, tibiofemoral articular cartilage must withstand compressive loads of multiple times body weight (Kutzner et al., 2010). The substantial load-bearing capacity of this multiphase tissue is provided by complex interactions between its solid network of collagen fibers and macromolecules, and the interstitial fluid. In an unloaded state, an electrostatic attraction between the proteoglycan macromolecules and the interstitial fluid leads to an osmotic pressurization of the tissue. This internal pressure is equilibrated by tensile loading in the collagen fibers. When cartilage is compressed, the contact loads are distributed throughout the tissue via further pressurization of the interstitial fluid (Cohen et al., 1998; Sophia Fox et al., 2009). This combination of interstitial fluid pressure and compressive and shearing contact loads results in a complex loading environment for the collagen fibers (Briant et al., 2015; Kääl et al., 1998; Notzli and Clark, 1997). Characterization of this collagen fiber loading during functional movement is critical to understand the superficial cartilage degradation and fibrillation associated with the initiation of osteoarthritis (Andriacchi et al., 2004; Carter et al., 2004; Griffin and Guilak, 2005; Poole et al., 2002).

Collagen fibers exhibit distinct patterns in orientation throughout the cartilage tissue. In the depth-wise direction, fibers extend vertically from the subchondral bone, bend through the mid-layer and lie parallel to the articular surface in the superficial layer (Benninghoff, 1925). Within the superficial layer, the fibers exhibit preferential orientation along the articular surface as well. This superficial collagen fiber orientation is revealed through split lines produced by inserting a needle coated in India ink into the tissue (Below et al., 2002; Benninghoff, 1925; Meachim et al., 1974; Responde et al., 2007).

Many researchers have proposed that the orientation of collagen fibers reflect a mechanobiologic adaptation to the local loading environment (Meachim et al., 1974; Responde et al., 2007). Yet, because measurement of internal cartilage loading is currently infeasible, investigating the relationship between fiber orientation and loading remains challenging. Commonly, finite element (FE) analysis is employed to estimate loading, however given the intricacy of the cartilage microstructure and its interactions, the development of high fidelity models continues to be an area of active research. Increasingly complex constitutive models of cartilage have been introduced to more accurately capture the response of cartilage to applied loads, including linear elastic, multiphase, and fibril reinforced (Halloran et al., 2012; Julkunen et al., 2013; Klika et al., 2016). Using these formulations, previous researchers simulated collagen remodelling based on mechanical parameters such as the principal strain directions to predict fiber alignment in the depth-wise direction (Cortez et al., n.d.; Wilson et al., 2006). Other researchers introduced pre-assumed cartilage split line orientations in fiber reinforced finite element models to study their influence on predicted cartilage strain patterns (Li et al., 2016; Mononen et al., 2012; Shim et al., 2016). However, while these continuum based FE models accurately capture the net mechanical response of cartilage (Julkunen et al., 2013) and provide insight into the mechanical effects of collagen fiber orientation, they do not provide a biomechanical explanation for the characteristic collagen fiber orientations that are observed in the cartilage surface.

Recent advancements in coupled multibody and finite element techniques, modeling of fluid-solid interaction, and large scale parallel simulation algorithms provide opportunity for high fidelity simulation of the loading of internal cartilage structures. When used with high performance computing clusters, computational physics engines such as Project Chrono (Mazhar et al., 2013; Tasora et al., 2016) enable simulations involving millions of discrete bodies. Thus, in the future, we envision multiscale cartilage models where collagen fibers are discretely modeled as deformable absolute nodal coordinate formulation (ANCF) beams (Shabana, 1997), the interstitial water is modeled with smoothed particle hydrodynamics (SPH) (Gingold and Monaghan, 1977), and the articular surface is modeled with ANCF shell elements (Yamashita et al., 2015a, 2015b). When coupled with a muscle-driven simulation, such a cartilage model will enable researchers to examine the relationship between loading of individual structures and mechanobiologic adaptation or the initiation and progression of osteoarthritis.

In this study, we introduce a multiscale simulation framework to predict superficial cartilage loading as a first step towards realizing this vision. This two-step simulation framework integrates kinematic and kinetic measurements of full body movement with a muscle-driven model of the knee joint to predict tibiofemoral kinematics during walking. These kinematics are then imposed on a knee model with deformable cartilage surfaces, represented by ANCF shell elements, to predict superficial cartilage mechanics. To demonstrate the capability of this simulation framework, cartilage surface strains are predicted due to passive osmotic pressure, a simulated walking cycle, and the combination of pressure and gait loading. The orientation of the principal strains in the cartilage surface resulting from these three conditions are compared against split lines maps from the literature to provide insight into the connection between collagen fiber loading and orientation.

Methods

Musculoskeletal Simulation to Predict Tibiofemoral Kinematics

A three-body (femur, tibia, patella), 12 degree-of-freedom (DOF) knee model was developed from magnetic resonance (MR) images of a healthy adult female (1.65 m, 61kg). Details of model development have been previously published (Lenhart et al., 2015), but will be briefly summarized for clarity. Fourteen ligaments were represented by bundles of nonlinear elastic springs, with wrapping surfaces included to prevent penetration of bony geometries. Articular cartilage surfaces were segmented from the MR images and represented by high resolution triangular meshes. Cartilage contact pressures were calculated based on the overlap depth between the articulating surfaces using an elastic foundation model (Bei and Fregly, 2004; Colin R. Smith et al., 2016b). The knee model was integrated into an existing lower extremity musculoskeletal model (Arnold et al., 2010), which included 43 muscles acting about the hip, knee and ankle joints. The predictive capacity of the model was validated by comparing simulated passive and active knee kinematics with in vivo 3D knee kinematics measured with dynamic MRI (Lenhart et al., 2015).

Tibiofemoral kinematics during walking were predicted using the Concurrent Optimization of Muscle Activations and Kinematics (COMAK) simulation routine (Colin R. Smith et al., 2016; Colin R. Smith et al., 2016a). Whole body kinematics and ground reactions were

recorded while the subject walked overground in a motion analysis laboratory. At each time step, numerical optimization was performed to calculate the muscle forces, patellofemoral kinematics and secondary tibiofemoral kinematics (5 DOF aside from flexion) that minimized the weighted sum of squared muscle activations while satisfying overall dynamic constraints. The constraints required that the muscle forces and internal knee loads (contact pressures and ligament forces) produced by the optimized knee kinematics generated the measured hip, knee (flexion) and ankle accelerations.

Deformable Cartilage Model

Using the geometries from the aforementioned model, a deformable model of the articular cartilage was developed to simulate the loading mechanics within the superficial layer. The cartilage surface was modeled with shell elements using a nonlinear finite element method: the absolute nodal coordinate formulation (ANCF). This formulation describes translations, rotations, and deformation using position vector and position vector gradient Lagrangian coordinates referred to an inertial reference frame (Shabana, 1997). ANCF naturally captures large displacements, large rotations, and moderate deformations which may occur in the cartilage. The element used in this study is a four node bilinear, continuum-based shell element, which was recently developed in (Yamashita et al., 2015a, 2015b). The shell element geometry is described by the position of its nodes and a position vector gradient defined to be oriented along the shell fiber over the thickness (Figure 2). An arbitrary point in the shell element is defined as a function of the global position of the nodes, \mathbf{r}^i , and its transverse gradient vector $\mathbf{r}_z^i = \frac{\partial \mathbf{r}^i}{\partial z^i}(x^i, y^i)$, which describes shear deformation. Element r 's positions and gradients on the mid-plane can be fully defined as:

$$\mathbf{r}_m^i(x^i, y^i) = \mathbf{S}_m^i(x^i, y^i)\mathbf{e}_p^i, \quad \cdot \cdot \cdot \quad \frac{\partial \mathbf{r}^i}{\partial z^i}(x^i, y^i) = \mathbf{S}_g^i(x^i, y^i)\mathbf{e}_g^i \quad (1)$$

where x^i and y^i refer to element r 's local coordinates, $\mathbf{S}_m^i = [\mathbf{S}_1^i \mathbf{I} \quad \mathbf{S}_2^i \mathbf{I} \quad \mathbf{S}_3^i \mathbf{I} \quad \mathbf{S}_4^i \mathbf{I}]$ is a bilinear shape function matrix, $\mathbf{e}_p^{ik} = \mathbf{r}^{ik}$ is the position vector of node k of element i , and $\mathbf{e}_g^{ik} = \frac{\partial \mathbf{r}^{ik}}{\partial z^i}$ is the position vector gradient of node k of element i . Shape functions are given by the following polynomials in local coordinates:

$$\begin{aligned} \mathbf{S}_1^i &= \frac{1}{4}(1-x^i)(1-y^i), \quad \mathbf{S}_2^i = \frac{1}{4}(1+x^i)(1-y^i), \\ \mathbf{S}_3^i &= \frac{1}{4}(1+x^i)(1+y^i), \quad \text{and } \mathbf{S}_4^i = \frac{1}{4}(1-x^i)(1+y^i) \end{aligned}$$

The position of an arbitrary point in the shell may be described as

$$\mathbf{r}^i(x^i, y^i, z^i) = \mathbf{S}^i(x^i, y^i, z^i)\mathbf{e}^i \quad (2)$$

where the combined shape function matrix is given by $\mathbf{S}^i = [\mathbf{S}_m^i \quad z^i \mathbf{S}_m^i]$. Positions and gradients may be combined as $\mathbf{e}^i = \left[(\mathbf{e}_p^i)^T (\mathbf{e}_g^i)^T \right]^T$. Note that Eq. (2) defines a volume, thereby allowing for continuum mechanics approaches to the internal force description. Using this description of element kinematics, the Green-Lagrange strain tensor may be obtained as $\mathbf{E}^i = \frac{1}{2}((\mathbf{F}^i)^T \mathbf{F}^i - \mathbf{I})$, where \mathbf{F}^i is the deformation gradient tensor defined as the current configuration over a reference configuration. Using the current absolute nodal coordinates, this tensor may be defined as $\mathbf{F}^i = \frac{\partial \mathbf{r}^i}{\partial \mathbf{X}^i} = \frac{\partial \mathbf{r}^i}{\partial \mathbf{x}^i} \left(\frac{\partial \mathbf{X}^i}{\partial \mathbf{x}^i} \right)^{-1}$ where the initial configuration of the articular cartilage surface, \mathbf{X}^i , is considered as reference. Numerical techniques are used to alleviate shear and thickness lockings in the element. Namely, assumed natural strains and enhanced strains, which find justification in the mixed variational principle by Hu–Washizu (Andelfinger and Ramm, 1993), are added to guarantee accuracy. Details on the software implementation and its verification may be consulted in (Peterson and Recuero, 2016; Recuero and Negrut, 2016).

The contribution of the underlying cartilage was represented using a combination of compressive spring-damper elements and internal pressure. A spring-damper element ($k = 0.7 \frac{N}{mm^3}$, $c = 7 \times 10^6 N \cdot \frac{s}{mm^3}$) was attached from each node of the ANCF shell elements to the surface of the underlying bone to model the compressive stiffness and the viscoelastic behaviour of the cartilage. The orientation and resting length of each spring-damper was determined by projecting the node transverse gradient vector, \mathbf{e}_g^i , in the reference configuration (\mathbf{X}^i) to the underlying bone. To model the osmotic pressurization of the cartilage, a constant pressure of 0.2 MPa (Ateshian et al., 2013; Chahine et al., 2005) was applied to the internal surface of the shell elements.

Contact Methods

Contact detection in the deformable cartilage surface model relied on triangularization of quad meshes, where each quad (ANCF shell) element is split into two triangles, thereby defining vertices, faces, and edges (Figure 3). A two-phase collision detection algorithm was implemented, where a broad phase rapidly determines potential contact pairs, which are then precisely evaluated for collision in a narrow phase. The shell element meshes were checked for contact by evaluating interpenetrations between vertices and faces, and between edges and edges. If contact is likely to occur, geometrical information, such as location of the contact point, normal direction, interpenetration, and interpenetration velocity are calculated for each vertex-face and edge-edge pair. A penalty formulation was used to generate normal forces; to ensure the desired accuracy, contact stiffness parameters and time steps were selected such that the maximum mesh interpenetration was at least one order of magnitude smaller than the calculated deflection of articular cartilage surfaces.

Simulation of Superficial Cartilage Mechanics

To simulate the loading in the superficial cartilage layer during walking, the predicted kinematics from the musculoskeletal simulation (§2.1) were imposed on the tibiofemoral

joint and the loading in the cartilage evolved naturally (Figure 1). The model was implemented in Chrono, an open-source, multi-physics software distributed under a BSD3 license and available online (Mazhar et al., 2013; Tasora et al., 2016). The bones were modelled as rigid bodies while the articular surfaces of the cartilage were modelled as deformable ANCF shell elements and were constrained to their corresponding bones at the periphery (§2.2). Contact between the deformable surfaces was handled via a penalty approach (§2.3). An implicit numerical time integration algorithm based on the Hilber-Hughes-Taylor (HHT) method was used to enable large time steps. Calculation of the Jacobian and the internal forces of the ANCF shell elements leveraged the multi-core shared-memory architecture of workstations via OpenMP. The resulting linear system of equations at each time step was solved by the Intel Math Kernel Library (MKL). The simulation of one gait cycle required 12 hours using 4 cores of an Intel Xeon Processor E5-2650 v3 25M Cache, 2.30 GHz.

Comparison with Cartilage Split Lines

To investigate the relationship between cartilage loading and collagen fiber orientation, the predicted first principal strain directions in the superficial layer of the femoral cartilage were qualitatively compared with experimental collagen fiber orientation (split line) maps from the literature (Below et al., 2002). Two-dimensional projections of the model were created to match the views of split line maps, and the magnitude-weighted time-averaged first principal strain directions throughout the simulation were computed at each node. Then, the split line maps were deformed using a non-rigid image transformation, Coherent Point Drift (Myronenko and Song, 2010), such that the outlines of the split line maps matched those of the model. The predicted strains were then spatially averaged to match the locations and the resolution of the experimental split line data. Finally, the deformed split line maps were visually compared against cartilage surface strains predicted for three loading conditions: i) osmotic pressurization, ii) a simulated gait cycle, iii) a gait cycle with osmotic pressurization.

Results

Verification of Joint Contact Forces and Cartilage Deflection

The deformable-surface model was verified by comparing i) tibiofemoral contact forces and ii) deflection of the femur and tibia cartilages obtained from the deformable-surface model against those predicted by the solid-surface model within the musculoskeletal simulation (Figure 4). Predicted tibiofemoral contact forces exhibited the characteristic double peak during stance, with the majority of the force passing through the medial compartment (Figure 5). The time-averaged root-mean-square (RMS) difference between the deformable-surface model and the solid-surface model for the net tibia plateau force in the superior-inferior (F_z) direction was 17%. The femoral cartilage deflection in the deformable-surface model was more evenly distributed in the contact region in comparison with the solid-surface model during mid-stance (Figure 6).

Prediction of Superficial Cartilage Deflection and Strain

The largest femoral cartilage deformation (1.1 mm) occurred in the medial compartment at the first peak of tibiofemoral loading (Figure 7). Correspondingly, the largest tensile and compressive strains occurred at the same time point, with magnitudes of 3% and -1%, respectively. During the gait cycle, the largest first principal strains, ϵ_{max} , were observed at the periphery of the contact region, while the principal strains were smaller and even negative (i.e. compressive) in the center of the contact region (Figure 7, middle column).

Comparison of Principal Strain and Collagen Fiber Directions

Three scenarios were simulated to investigate the connection between cartilage split line orientations and loading: i) osmotic pressure, ii) walking and iii) combined osmotic pressure and walking (Figure 8). In general, the principal strain directions of the two scenarios which include internal osmotic pressure exhibit good agreement with the experimental split line orientations, with a notable exception on the posterior aspect of the medial condyle.

Discussion

In this study, we introduced a two-step simulation framework consisting of a musculoskeletal simulation to predict six degree of freedom tibiofemoral kinematics and a deformable-surface simulation to predict loading in the superficial layer of the tibiofemoral cartilage. The deformable-surface model employs finite element ANCF shells to simulate principal strain directions in the articular surface, where collagen fibers exhibit characteristic orientation patterns (Below et al., 2002). The simulation framework was used to predict superficial cartilage strains due to passive osmotic pressure, a walking cycle, and combined osmotic pressure and walking. The orientations of the principal strains for each of these scenarios were compared to cartilage split line patterns to investigate the mechanobiologic connection proposed by previous researchers (Meachim et al., 1974; Responde et al., 2007). These comparisons revealed the importance of including the passive osmotic pressure within the cartilage model to pre-strain the superficial layer.

The presented simulation framework is an important step towards simulation of detailed cartilage microstructure loading during movement. Our framework differs from conventional sequential frameworks in both the musculoskeletal simulation and detailed cartilage model. The movement simulation is performed using the COMAK algorithm, which simultaneously solves the musculoskeletal movement dynamics and internal joint mechanics (Colin R. Smith et al., 2016; Colin R. Smith et al., 2016a). This ensures dynamic consistency and allows prediction of secondary joint kinematics which cannot be readily measured using motion capture. In the deformable-surface cartilage model, the use of an ANCF shell representation of the cartilage surface enables detailed prediction of loading in the superficial cartilage layer. The ANCF formulation in Chrono enables straightforward interfacing of a more detailed model of the underlying cartilage with explicit representation of the collagen fibers (ANCF beams) and ionic fluid (SPH) to be implemented in the future.

Our predictions of cartilage mechanics during walking are consistent with indirect experimental measures. Similar to studies which measured cartilage thickness before and

after walking (Lad et al., 2016), and combined biplane fluoroscopy and MR based models (Liu et al., 2010), we found substantially larger deformation in the medial compartment. Furthermore, considering the cartilage was approximately 4 mm thick in the contact region, our predicted maximum deflection (1.1mm) at the first peak tibiofemoral load during gait corresponds favourably with ~25% deformation measured by (Liu et al., 2010) and estimated by (Shim et al., 2016).

The comparison of predicted cartilage principal strain directions and experimental cartilage split line orientations revealed several insights. First, the principal strain directions induced solely by the resting osmotic pressure corresponded well with the experimental split lines (Figure 8). This provides a simple method to approximate collagen fiber orientations, and therefore anisotropic cartilage surface properties, for subject-specific models, without relying upon a limited database of split-line maps (Below et al., 2002; Benninghoff, 1925; Meachim et al., 1974) or simple geometric assumptions as employed by previous researchers (Mononen et al., 2012; Shim et al., 2016). Second, the predicted strain directions resulting from a simulated walking cycle showed much better agreement with split line patterns when the osmotic pressure was included. This highlights the importance of including pre-strain in the articular surface, and reinforces the need for higher fidelity models of the underlying cartilage which can explicitly model the components of the extracellular matrix and capture fluid-solid and electromechanical interactions (Ateshian et al., 2013).

Our results agree with previous simulation studies, indicating that there is likely a connection between loading and collagen fiber orientation. These studies suggest that superficial cartilage strain is reduced along the split line directions, and that stress is greater when collagen fibers are randomly oriented (Mononen et al., 2012; Shim et al., 2016). Experimental findings support this result, as the tensile strength of cartilage is greatest when measured parallel to the collagen fiber direction (Kempson et al., 1973; Sasazaki et al., 2006). Although the physiologic mechanism linking collagen orientation to loading is still uncertain, an enzyme that selectively degrades unloaded collagen fibers may provide this link (Nabeshima et al., 1996; Ruberti and Hallab, 2005). There are two mechanisms which load collagen fibers: the resting osmotic fluid pressure and the compression induced by functional movements (Sophia Fox et al., 2009). While the previous simulation studies have focused solely on the latter, the results of this study indicate that the contribution of osmotic pressure should not be over looked.

References

- Andelfinger U, Ramm E, 1993 EAS-elements for two-dimensional, three-dimensional, plate and shell structures and their equivalence to HR-elements. *Int. J. Numer. Methods Eng.* 36, 1311–1337. doi: 10.1002/nme.1620360805
- Andriacchi TP, Mündermann A, Smith RL, Alexander EJ, Dyrby CO, Koo S, 2004 A framework for the in vivo pathomechanics of osteoarthritis at the knee. *Ann. Biomed. Eng.* 32, 447–57. [PubMed: 15095819]
- Arnold EM, Ward SR, Lieber RL, Delp SL, 2010 A Model of the Lower Limb for Analysis of Human Movement. *Ann. Biomed. Eng.* 38, 269–279. doi:10.1007/s10439-009-9852-5 [PubMed: 19957039]
- Ateshian GA, Maas S, Weiss JA, 2013 Multiphasic finite element framework for modeling hydrated mixtures with multiple neutral and charged solutes. *J. Biomech. Eng.* 135, 111001. doi: 10.1115/1.4024823 [PubMed: 23775399]

- Bei Y, Fregly BJ, 2004 Multibody dynamic simulation of knee contact mechanics. *Med.Eng Phys.* 26, 777–789. [PubMed: 15564115]
- Below S, Arnoczky SP, Dodds J, Kooima C, Walter N, 2002 The split-line pattern of the distal femur: A consideration in the orientation of autologous cartilage grafts. *Arthroscopy* 18, 613–617. doi: 10.1053/jars.2002.29877 [PubMed: 12098122]
- Benninghoff A, 1925 Form und Bau der Gelenkknorpel in ihren Beziehungen zur Funktion. *Z. Anat. Entwicklungsgesch.* 76, 43–63. doi:10.1007/BF02134417
- Briant P, Bevell S, Andriacchi T, 2015 Cartilage Strain Distributions are Different under the Same Load in the Central and Peripheral Tibial Plateau Regions. *J. Biomech. Eng.* 137, 1–7. doi: 10.1115/1.4031849
- Carter DR, Beaupré GS, Wong M, Smith RL, Andriacchi TP, Schurman DJ, 2004 The mechanobiology of articular cartilage development and degeneration. *Clin. Orthop. Relat. Res.* S69–S77. doi: 00003086-200410001-00014 [pii] [PubMed: 15480079]
- Chahine NO, Chen FH, Hung CT, Ateshian G a, 2005 Direct measurement of osmotic pressure of glycosaminoglycan solutions by membrane osmometry at room temperature. *Biophys. J.* 89, 1543–50. doi:10.1529/biophysj.104.057315 [PubMed: 15980166]
- Cohen NP, Foster RJ, Mow VC, 1998 Composition and Dynamics of Articular Cartilage: Structure, Function, and Maintaining H ealthy State. *J. Orthopadic Sport. Phys. Ther.* 28, 203–215. doi: 10.2519/jospt.1998.28.4.203
- Cortez S, Completo A, Alves JL, n.d. A novel computational modelling to describe the anisotropic, remodelling and reorientation behaviour of collagen fibres in articular cartilage. *arXiv Prepr. arXiv1601.05295* (2016).
- Gingold RA, Monaghan JJ, 1977 Smoothed particle hydrodynamics: theory and application to non-spherical stars. *Mon. Not. R. Astron. Soc.* 181, 375–389. doi:10.1093/mnras/181.3.375
- Griffin TM, Guilak F, 2005 The role of mechanical loading in the onset and progression of osteoarthritis. *Exerc. Sport Sci. Rev.* 33, 195–200. doi:10.1097/00003677-200510000-00008 [PubMed: 16239837]
- Halloran JP, Sibole S, van Donkelaar CC, van Turnhout MC, Oomens CWJ, Weiss J a, Guilak F, Erdemir a, 2012 Multiscale mechanics of articular cartilage: potentials and challenges of coupling musculoskeletal, joint, and microscale computational models. *Ann. Biomed. Eng.* 40, 2456–74. doi:10.1007/s10439-012-0598-0 [PubMed: 22648577]
- Julkunen P, Wilson W, Isaksson H, Jurvelin JS, Herzog W, Korhonen RK, 2013 A Review of the Combination of Experimental Measurements and Fibril-Reinforced Modeling for Investigation of Articular Cartilage and Chondrocyte Response to Loading 2013.
- Kääb MJ, Ito K, Clark JM, Nötzli HP, 1998 Deformation of articular cartilage collagen structure under static and cyclic loading. *J. Orthop. Res.* 16, 743–51. doi:10.1002/jor.1100160617 [PubMed: 9877400]
- Kempson GE, Muir H, Pollard C, Tuke M, 1973 The tensile properties of the cartilage of human femoral condyles related to the content of collagen and glycosaminoglycans. *Biochim. Biophys. Acta* 297, 456–72. doi:10.1016/0304-4165(73)90093-7 [PubMed: 4267503]
- Klika V, Gaffney EA, Chen Y-C, Brown CP, 2016 An overview of multiphase cartilage mechanical modelling and its role in understanding function and pathology. *J. Mech. Behav. Biomed. Mater.* 62, 139–57. doi:10.1016/j.jmbbm.2016.04.032 [PubMed: 27195911]
- Kutzner I, Heinlein B, Graichen F, Bender a, Rohlmann a, Halder a, Beier a, Bergmann G, 2010 Loading of the knee joint during activities of daily living measured in vivo in five subjects. *J. Biomech.* 43, 2164–73. doi:10.1016/j.jbiomech.2010.03.046 [PubMed: 20537336]
- Lad NK, Liu B, Ganapathy PK, Utturkar GM, Sutter EG, Moorman CT, Garrett WE, Spritzer CE, DeFrate LE, 2016 Effect of normal gait on in vivo tibiofemoral cartilage strains. *J. Biomech.* doi: 10.1016/j.jbiomech.2016.06.025
- Lenhart RL, Kaiser J, Smith CR, Thelen DG, 2015 Prediction and Validation of Load-Dependent Behavior of the Tibiofemoral and Patellofemoral Joints During Movement. *Ann. Biomed. Eng.* 43, 2675–2685. doi:10.1007/s10439-015-1326-3 [PubMed: 25917122]

- Li J, Hua X, Jones AC, Williams S, Jin Z, Fisher J, Wilcox RK, 2016 The influence of the representation of collagen fibre organisation on the cartilage contact mechanics of the hip joint. *J. Biomech.* 49, 1679–1685. doi:10.1016/j.jbiomech.2016.03.050 [PubMed: 27079623]
- Liu F, Kozanek M, Hosseini A, Van de Velde SK, Gill TJ, Rubash HE, Li G, 2010 In vivo tibiofemoral cartilage deformation during the stance phase of gait. *J. Biomech.* 43, 658–65. doi:10.1016/j.jbiomech.2009.10.028 [PubMed: 19896131]
- Mazhar H, Heyn T, Pazouki A, Melanz D, Seidl A, Bartholomew A, Tasora A, Negrut D, 2013 CHRONO: a parallel multi-physics library for rigid-body, flexible-body, and fluid dynamics. *Mech. Sci.* 4, 49–64. doi:10.5194/ms-4-49-2013
- Meachim G, Denham D, Emery IH, Wilkinson PH, 1974 Collagen alignments and artificial splits at the surface of human articular cartilage. *J. Anat.* 118, 101–18. [PubMed: 4426874]
- Mononen ME, Mikkola MT, Julkunen P, Ojala R, Nieminen MT, Jurvelin JS, Korhonen RK, 2012 Effect of superficial collagen patterns and fibrillation of femoral articular cartilage on knee joint mechanics-A 3D finite element analysis. *J. Biomech.* 45, 579–587. doi:10.1016/j.jbiomech.2011.11.003 [PubMed: 22137088]
- Myronenko A, Song X, 2010 Point set registration: coherent point drift. *IEEE Trans. Pattern Anal. Mach. Intell.* 32, 2262–75. doi:10.1109/TPAMI.2010.46 [PubMed: 20975122]
- Nabeshima Y, Grood ES, Sakurai A, Herman JH, 1996 Uniaxial tension inhibits tendon collagen degradation by collagenase in vitro. *J. Orthop. Res.* 14, 123–130. doi:10.1002/jor.1100140120 [PubMed: 8618154]
- Notzli H, Clark J, 1997 Deformation of loaded articular cartilage prepared for scanning electron microscopy with rapid freezing and freeze-substitution fixation. *J. Orthop. Res.* 15, 76–86. doi:10.1002/jor.1100150112 [PubMed: 9066530]
- Peterson B, Recuero A, 2016 Validation of a bilinear, gradient-deficient ANCF shell element in Chrono::FEA.
- Poole AR, Kobayashi M, Yasuda T, Laverty S, Mwale F, Kojima T, Sakai T, Wahl C, El-Maadawy S, Webb G, Tchetina E, Wu W, 2002 Type II collagen degradation and its regulation in articular cartilage in osteoarthritis. *Ann. Rheum. Dis.* 61, 78ii–81. doi:10.1136/ard.61.suppl_2.ii78
- Recuero A, Negrut D, 2016 Chrono Support for ANCF Finite Elements: Formulation and Validation Aspects.
- Responte DJ, Natoli RM, Athanasiou K a, 2007 Collagens of articular cartilage: structure, function, and importance in tissue engineering. *Crit. Rev. Biomed. Eng.* 35, 363–411. doi:10.1615/CritRevBiomedEng.v35.i5.20 [PubMed: 19392643]
- Ruberti JW, Hallab NJ, 2005 Strain-controlled enzymatic cleavage of collagen in loaded matrix. *Biochem. Biophys. Res. Commun.* 336, 483–489. doi:10.1016/j.bbrc.2005.08.128 [PubMed: 16140272]
- Sasazaki Y, Shore R, Seedhom BB, 2006 Deformation and failure of cartilage in the tensile mode. *J. Anat.* 208, 681–694. doi:10.1111/j.1469-7580.2006.00569.x [PubMed: 16761971]
- Shabana AA, 1997 Definition of the Slopes and the Finite Element Absolute Nodal Coordinate Formulation. *Multibody Syst. Dyn.* 1, 339–348. doi:10.1023/A:1009740800463
- Shim VB, Besier TF, Lloyd DG, Mithraratne K, Fernandez JF, 2016 The influence and biomechanical role of cartilage split line pattern on tibiofemoral cartilage stress distribution during the stance phase of gait. *Biomech. Model. Mechanobiol.* 15, 195–204. doi:10.1007/s10237-015-0668-y [PubMed: 25861029]
- Smith CR, Lenhart RL, Kaiser J, Vignos MF, Thelen DG, 2016 Influence of Ligament Properties on Tibiofemoral Mechanics in Walking. *J. Knee Surg.* 29, 99–106. doi:10.1055/s-0035-1558858 [PubMed: 26408997]
- Smith CR, Vignos MF, Lenhart RL, Kaiser J, Thelen DG, 2016a The Influence of Component Alignment and Ligament Properties on Tibiofemoral Contact Forces in Total Knee Replacement. *J. Biomech. Eng.* 138. doi:10.1115/1.4032464
- Smith CR, Won Choi K, Negrut D, Thelen DG, 2016b Efficient computation of cartilage contact pressures within dynamic simulations of movement. *Comput. Methods Biomech. Biomed. Eng. Imaging Vis.* 1163, 1–8. doi:10.1080/21681163.2016.1172346

- Sophia Fox AJ, Bedi A, Rodeo SA, 2009 The basic science of articular cartilage: structure, composition, and function. *Sports Health* 1, 461–8. doi:10.1177/1941738109350438 [PubMed: 23015907]
- Tasora A, Serban R, Mazhar H, Pazouki A, Melanz D, Fleischmann J, Taylor M, Sugiyama H, Negrut D, 2016 Chrono: An Open Source Multi-physics Dynamics Engine, in: *Lecture Notes in Computer Science (including Subseries Lecture Notes in Artificial Intelligence and Lecture Notes in Bioinformatics)*. pp. 19–49. doi:10.1007/978-3-319-40361-8_2
- Wilson W, Driessen NJB, van Donkelaar CC, Ito K, 2006 Prediction of collagen orientation in articular cartilage by a collagen remodeling algorithm. *Osteoarthr. Cartil.* 14, 1196–1202. doi:10.1016/j.joca.2006.05.006 [PubMed: 16797194]
- Yamashita H, Jayakumar P, Sugiyama H, 2015a Development of Shear Deformable Laminated Shell Element and its Application to ANCF Tire Model, in: *Volume 6: 11th International Conference on Multibody Systems, Nonlinear Dynamics, and Control*. ASME, p. V006T10A069. doi:10.1115/DETC2015-46173
- Yamashita H, Valkeapää AI, Jayakumar P, Sugiyama H, 2015b Continuum Mechanics Based Bilinear Shear Deformable Shell Element Using Absolute Nodal Coordinate Formulation. *J. Comput. Nonlinear Dyn.* 10, 051012. doi:10.1115/1.4028657

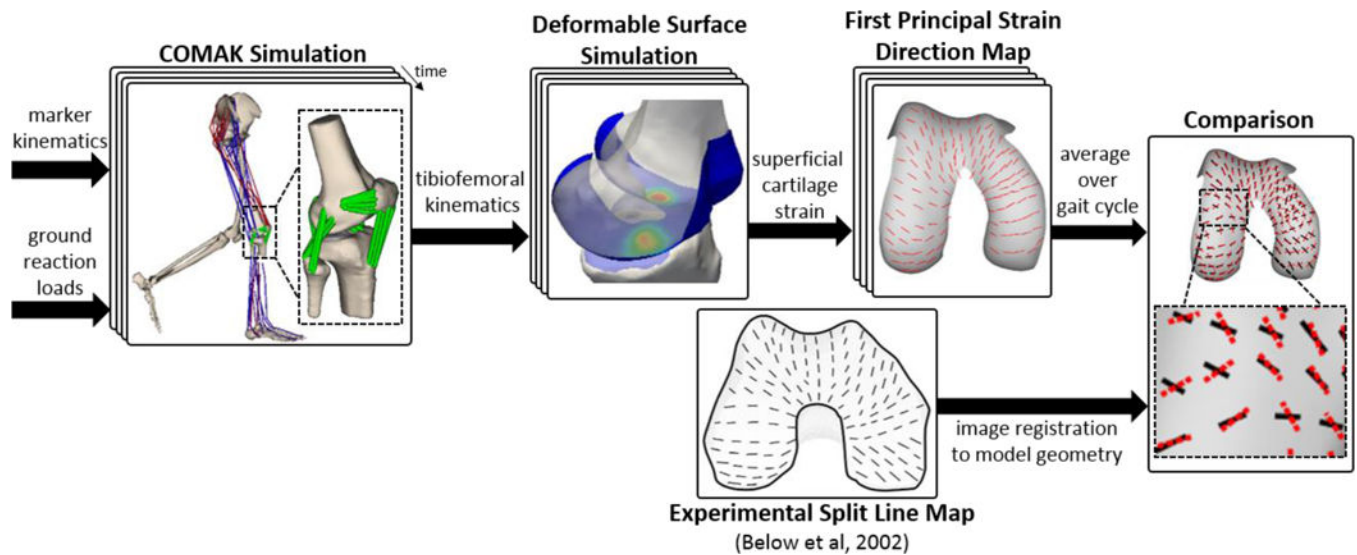


Figure 1:

Overview of the two-step simulation process. First, a musculoskeletal dynamic simulation (COMAK), including an elastic foundation contact model, was used to solve for tibiofemoral knee kinematics. Then, a novel deformable surface model was used to estimate superficial cartilage strain at each instant in the gait cycle. Finally, the average first principal strain directions were visually compared with experimental split line maps (Below et al., 2002) which represent collagen fiber alignment.

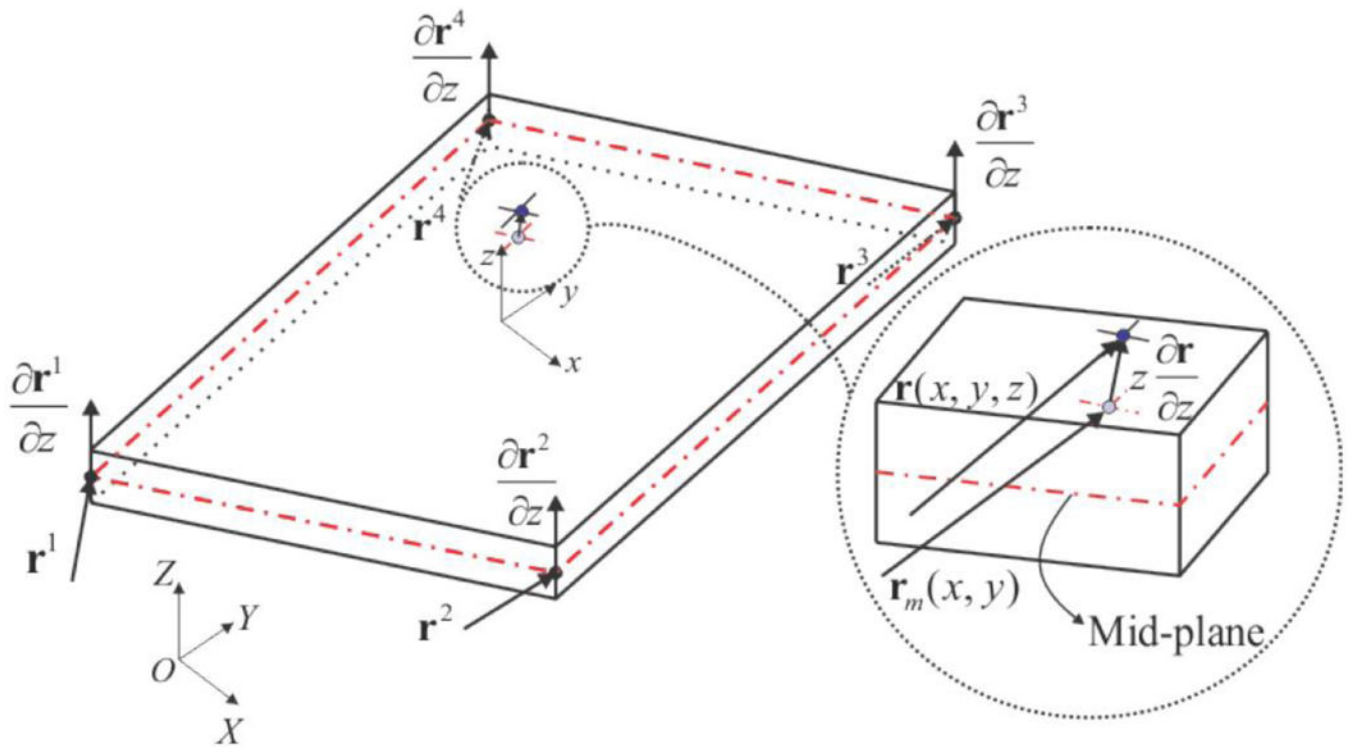


Figure 2: ANCF shell element's kinematic description. The global position of an arbitrary point on the element is defined by the local coordinates in the element frame (x, y, z) , and nodal global position ($e_p^k = r^k$) and transverse gradient ($e_g^k = \frac{\partial r^k}{\partial z}$) vectors. A close-up is provided to illustrate the definition of an arbitrary point $(r(x, y, z))$ from the mid-plane ($r_m(x, y)$) location and transverse gradient vector ($z \frac{\partial r}{\partial z}$)

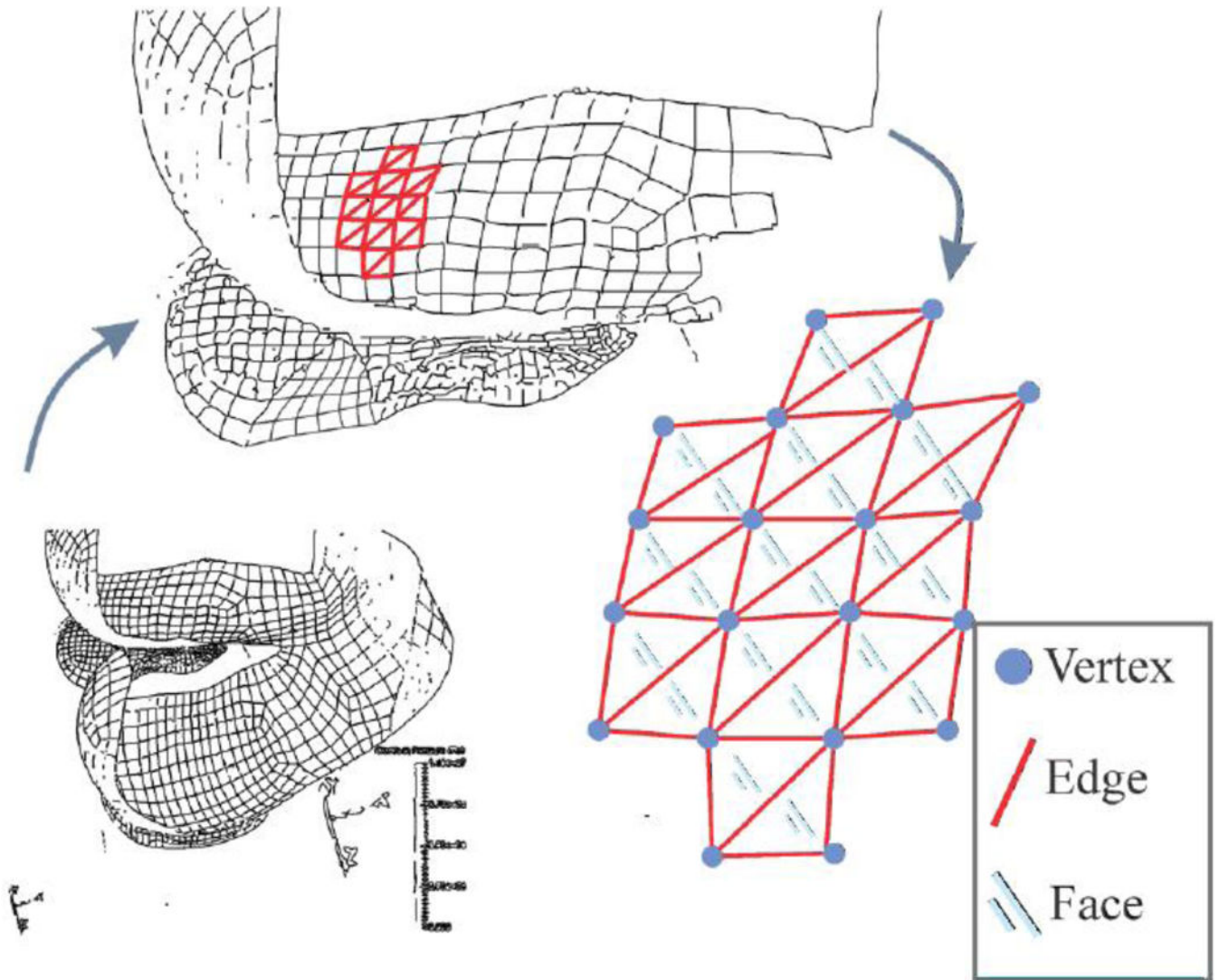


Figure 3: Triangular mesh for articular cartilage surface vs surface contact. The quad finite element mesh is first converted to a triangular mesh composed of vertices, edges, and faces. Each vertex is associated with a normal vector to compute interpenetrations.

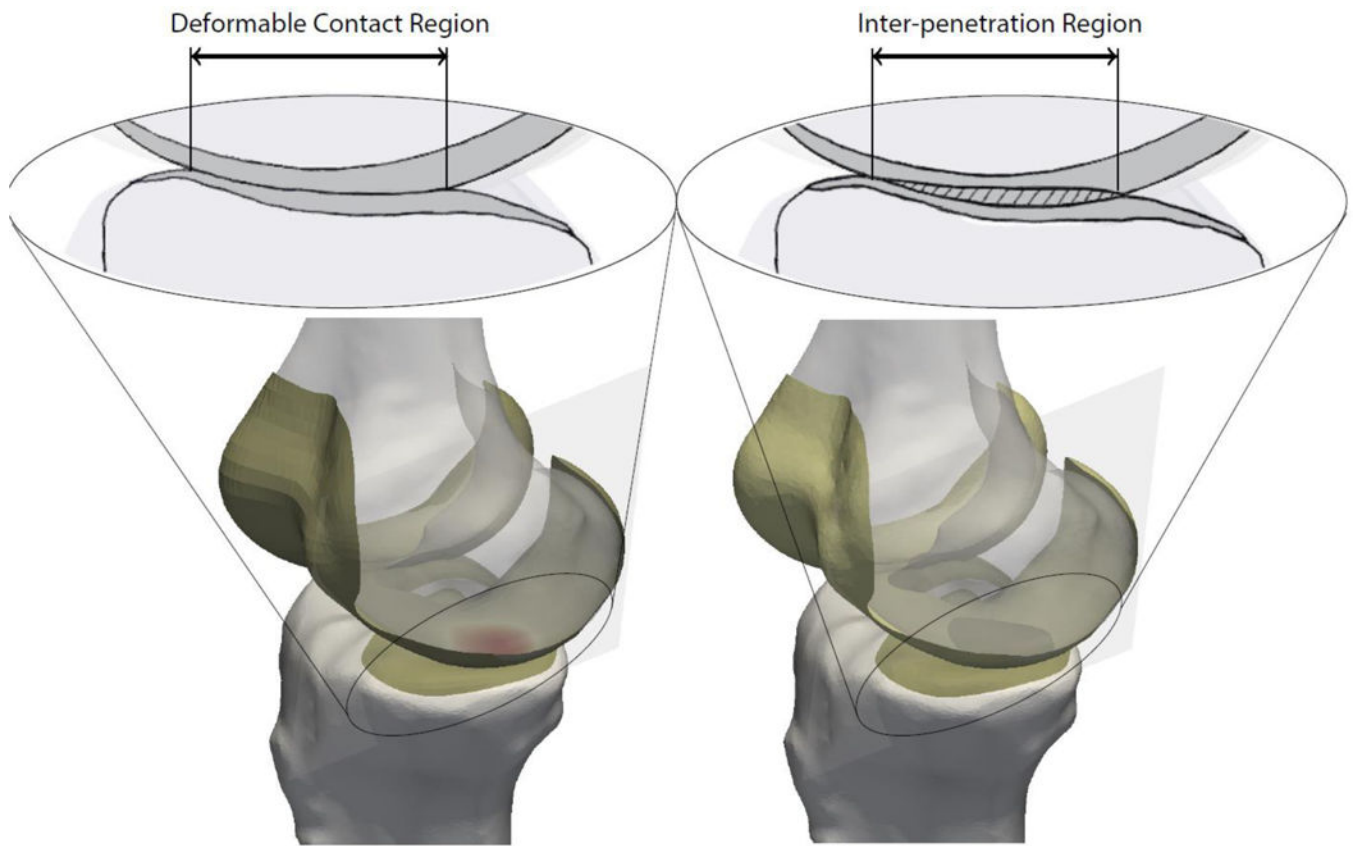


Figure 4: Schematic comparison of the deformable-surface model (left) with the solid-surface model (right) with the 2D section views on top.

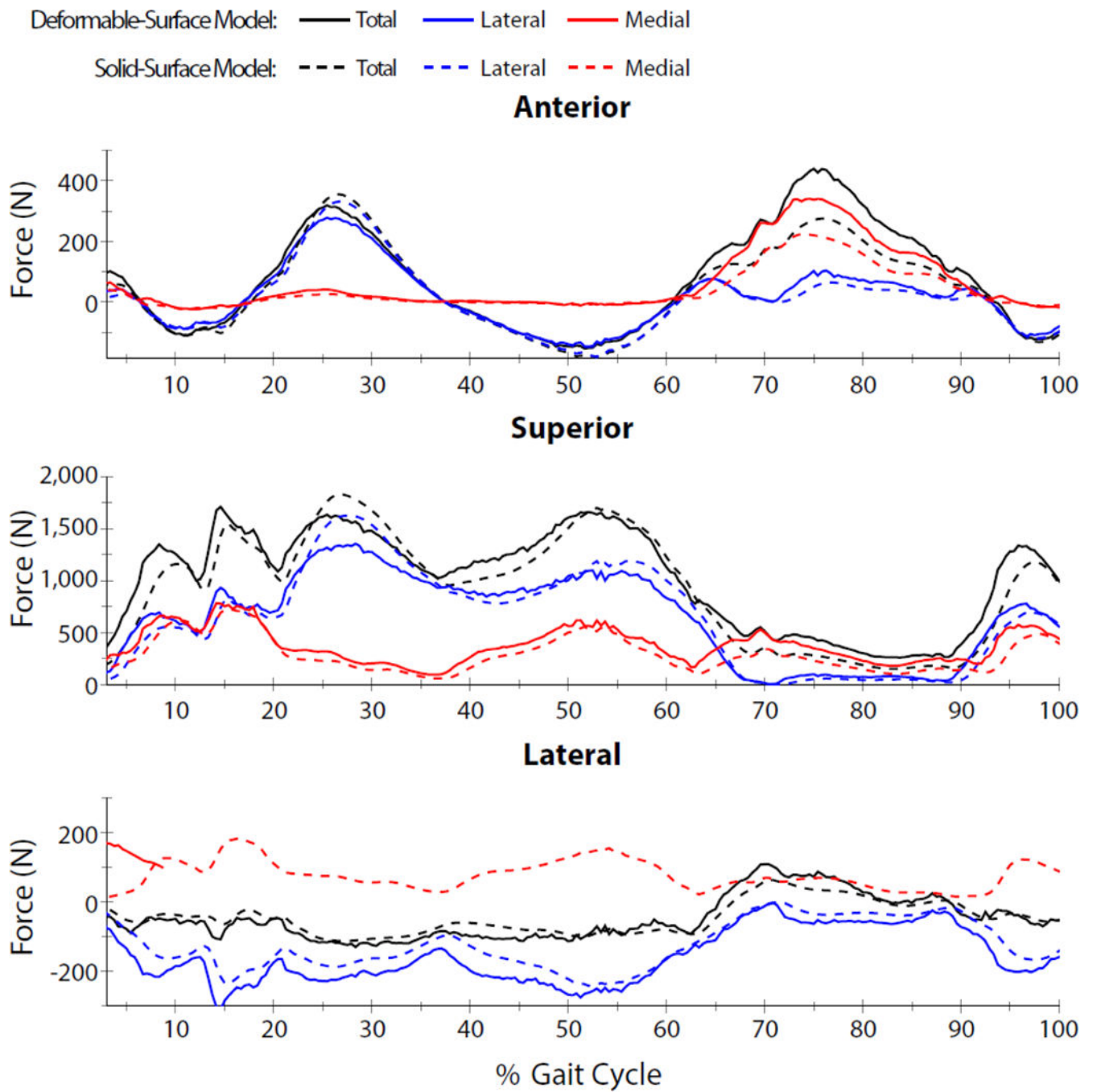


Figure 5: Comparison of the net load results on the femur, medial and lateral cartilages with the solid-surface model (Colin R. Smith et al., 2016b).

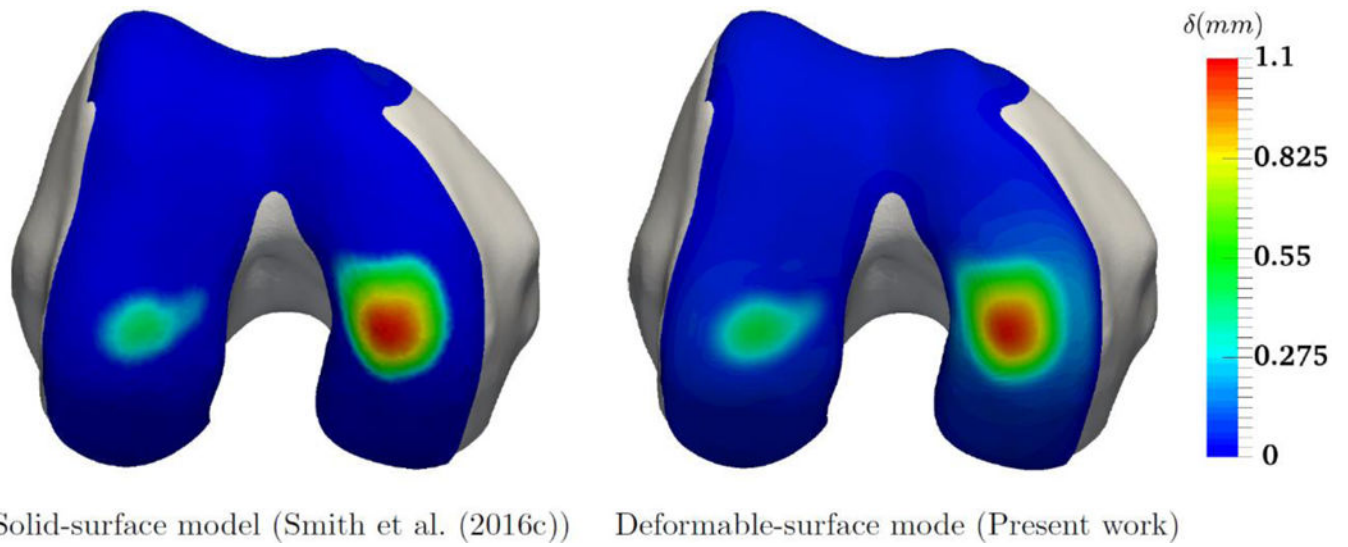


Figure 6:
Comparison of articular cartilage interpenetration (rigid model) and deflection (flexible model)

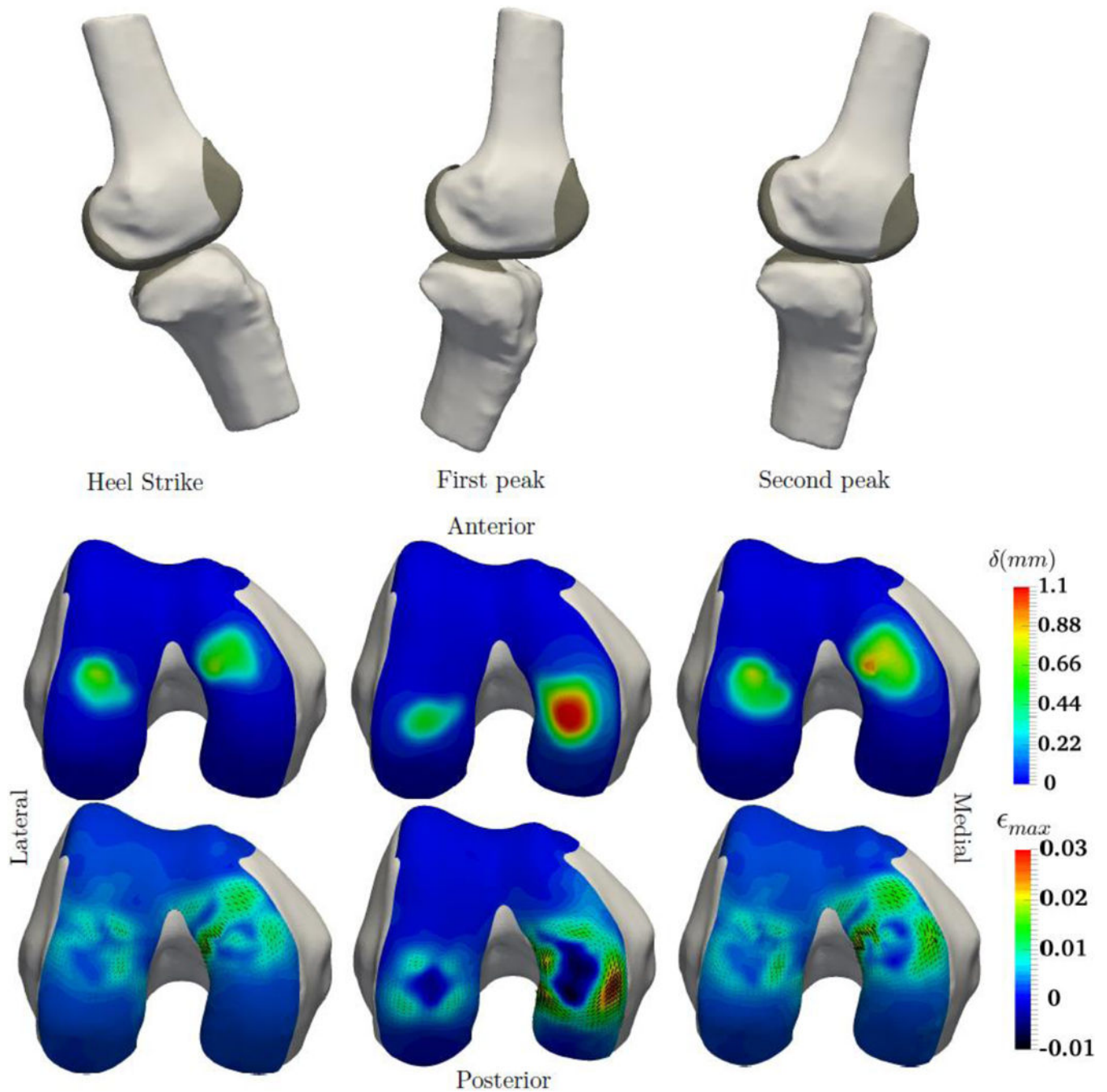


Figure 7: Different instants of time during the gait cycle when no internal pressure is applied. First row: schematic of the motion during the gait cycle. Second row: deflection field. Third row: maximum principal strains. Arrows show the first principal strain directions and are scaled by the magnitude of the first principal strain at each FE node. See Fig. 9 in supplementary information for corresponding tibial plateau pressures and strain patterns.

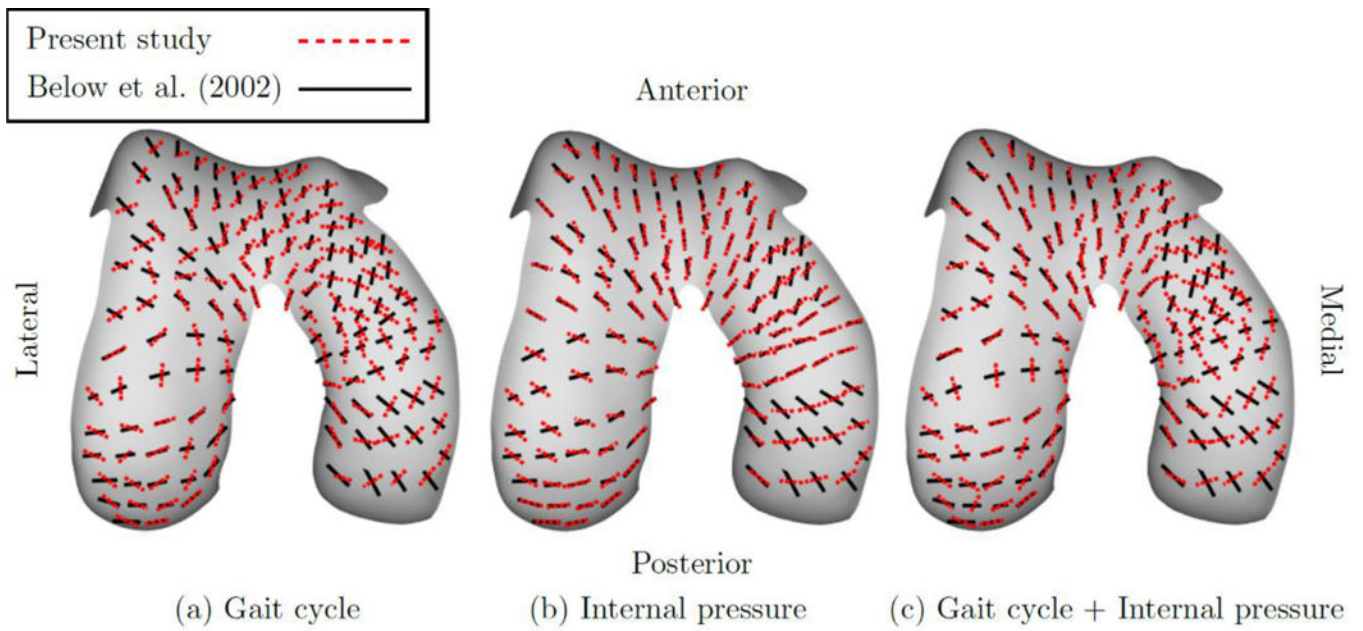


Figure 8:

Comparison of the fiber alignment predicted by this study for different scenarios with experimental results (Below et al. (2002a)) on the femur condyle. See Fig. 10 in supplementary information for simulated first principal strain directions on the tibial plateau..

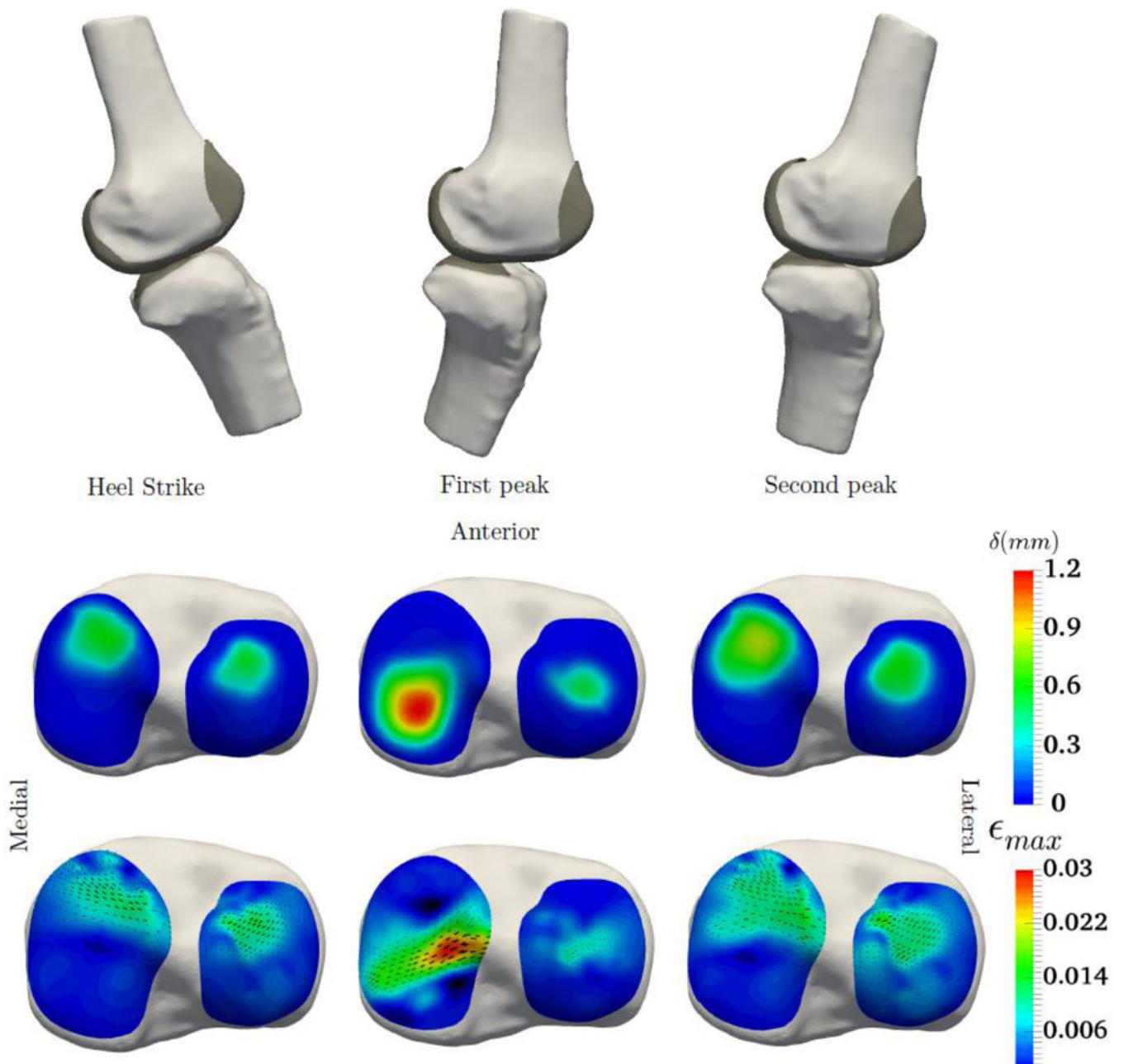


Figure 9:

Different instants of time during the gait cycle when no internal pressure is applied. First row: schematic of the motion during the gait cycle. Second row: deflection field. Third row: maximum principal strains (Arrows show the maximum principal strain directions and are scaled by the magnitude of the principal strain at each FE node).

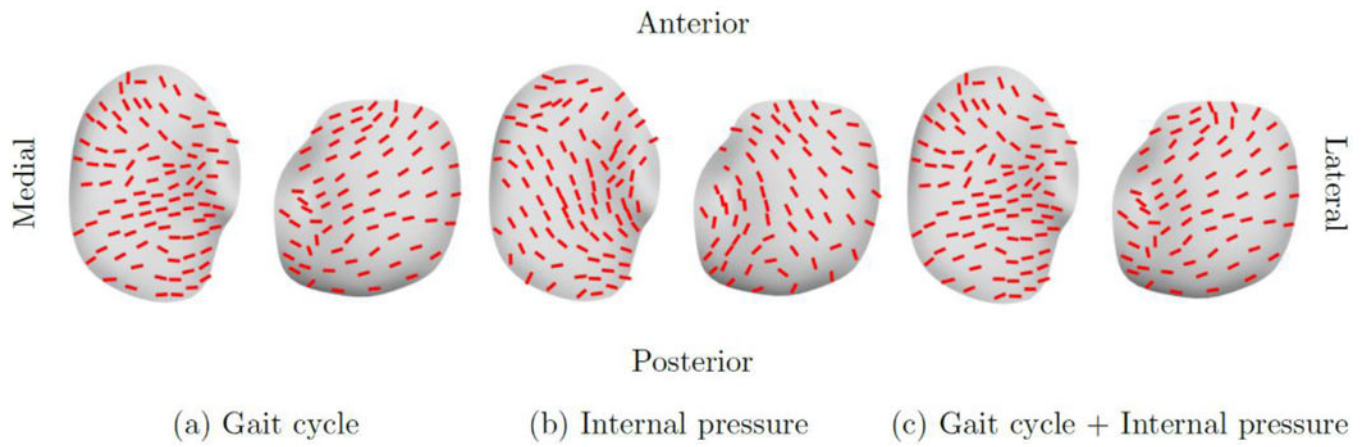


Figure 10: Comparison of the average first principal strain directions induced via (a) tibiofemoral loading during gait, (b) internal osmotic pressure and (c) coupled gait loading and osmotic pressure.